RSC Advances

PAPER

View Article Online
View Journal | View Issue

Cite this: *RSC Adv.*, 2018, **8**, 37375

Design, synthesis and characterization of novel chromone based-copper(II) antitumor agents with *N,N*-donor ligands: comparative DNA/RNA binding profile and cytotoxicity†

Farukh Arjmand, *[a] Zeenat Afsan [a] and Thierry Roisnel[b]

A series of new chromone based-Cu(II) complexes **1–3** derived from bioactive pharmacophore, 3-formylchromone and *N,N*-donor ligands *viz.*, 1,10-phenanthroline, 2,2′-bipyridine and 1*R*,2*R*-DACH were synthesized as potential antitumor agents and thoroughly characterized by UV-vis, FT-IR, EPR, ESI-MS and elemental analysis. Single X-crystal diffraction studies of complex **2** revealed triclinic $P\bar{1}$ space group with square pyramidal geometry around the Cu(II) center. Comparative *in vitro* binding studies with ct-DNA and tRNA were carried out using absorption and emission titration experiments which revealed intercalative mode of binding with higher binding propensity of complexes **1–3** towards tRNA as compared to ct-DNA. Additionally, complex **1** exhibited high binding affinity among all the three complexes due to the involvement of phen co-ligands *via* π-stacking interactions in between nucleic acid base pairs. Furthermore, Hirshfeld surface analysis was carried out for complex **2** to investigate various intra and intermolecular non-covalent interactions (H-bonding, C–H···π *etc.*) accountable for stabilization of crystal lattice. The cleavage activity of complex **1** was performed by gel electrophoretic assay with pBR322 DNA and tRNA which revealed efficient DNA/tRNA cleaving ability of complex, suggesting tRNA cleavage both concentration and time dependent. Furthermore, *in vitro* cytotoxic activity of complexes **1–3** on a selected panel of human cancer cell lines was performed which revealed that all three complexes exhibited remarkably good cytotoxic activity with GI_{50} value < 10 μg mL^{-1} (<20 μM).

Received 10th August 2018
Accepted 23rd October 2018

DOI: 10.1039/c8ra06722h

rsc.li/rsc-advances

Introduction

Copper – an essential metal ion (150 mg in the human body of an adult) with d^9 configuration is a cofactor for numerous enzymatic reactions that are crucial for life. Copper-coordinated complexes have attracted much attention owing to their unique biological,[1] spectroscopic[2] and catalytic properties.[3] Cu(II) exhibits strong and kinetically inert bonds with various chosen ligands in the biological environments such as imine-nitrogen atom in the imidazole ring of histidines or chelating atoms of polypyridyls. A wide range of copper complexes as cytotoxic agents have been explored, appearing in many review articles.[4,5] Literature reports reveal the importance of Cu in angiogenesis,[5] which plays a pivotal role in growth and development, in cell proliferation and metastasis of tumour.[6] As a matter of fact, copper complexes have met the criteria for design of efficacious drug candidates due to their potential to (i) interact strongly with biomolecules (ii) control the toxicity at trace levels and (iii) induce apoptosis [kills the cancerous cells without affecting the normal cells].

Keeping in mind the complexity of cancers which show diverse phenotypes and multiple etiologies, a "one-size-fits-all" drug design strategy for the development of cancer chemotherapeutics does not yield successful results. *In lieu* of this, copper(II)-based therapeutics with some naturally occurring compounds such as flavonoids, coumarins, chromones[7,8] *etc.* that could block/inhibit the cell proliferation pathway in a specific manner, are much desired. It has been demonstrated in literature that copper-based complexes are more potent antitumor agents than free metal salts or organic ligands. The cytotoxicity of complexes is highly dependent on ligand scaffold around the copper ion. Chromones have been demonstrated in the literature previously as privileged medicinal scaffold which have found application as an anti-inflammatory, antibacterial and anticancer agents.[9,10] Furthermore, chromone based drugs have been found to inhibit different types of cancer targets,[11] nucleic acids (DNA/RNA),[12,13] enzymes (kinase inhibitors and topoisomerases)[14] and other membrane receptors.[15]

[a]*Department of Chemistry, Aligarh Muslim University, Aligarh 202002, India. E-mail: farukh_arjmand@yahoo.co.in; Tel: +91 5712703893*

[b]*Institut des Sciences Chimiques de Rennes, UMR 6226, Université de Rennes 1, Campus de Beaulieu Bâtiment 10B, Bureau, 15335042 Rennes, France*

† Electronic supplementary information (ESI) available. CCDC 1574863. For ESI and crystallographic data in CIF or other electronic format see DOI: 10.1039/c8ra06722h

Many copper-chromone complexes have been investigated for their anticancer activity and most of the synthesised compounds showed improved cytotoxicities against different phenotypes of cancer cell lines with varied potencies.[16–19] In our laboratory, the cytotoxic potential of chromone-Cu(II) drug entity was validated on human breast (MCF-7) and liver cancer (HepG2) cell lines which revealed significantly lower IC_{50} values (5–10 μg mL^{-1}) for both cancer cell lines, which was much lower than the IC_{50} values of previously reported other similar Cu(II) complexes.[13] Recently, Prabhakaran *et al.* have synthesized chromone-based Cu(II) complexes and analysed their binding profile and cytotoxic activities.[16]

To further modulate the biological activity of the complexes, the incorporation of secondary ancillary ligands (hydrophobic/hydrophilic) is considered as a much desired option. In this work, *N*,*N*-donor ligand framework *viz.* 1,10-phenanthroline, 2,2′-bipyridine and 1*R*,2*R*-DACH were judicially chosen as they exhibit relatively higher affinity towards copper ion.[20,21] Moreover, the extended aromatic ring systems in 1,10-phenanthroline and 2,2′-bipyridine can induce facile intercalation/groove binding interaction with the base pairs of nucleic acids; on the other hand, DACH have been demonstrated to improve the pharmacological efficacy of platinum-based drug (oxaliplatin) significantly by inhibiting DNA mismatch repair and increasing cellular uptake.[22]

DNA is the primary target of several prominent metal-based anticancer drugs. However, recent studies have been focused on RNA as a drug target[23] as RNAs are highly structured with tertiary folding that are responsible for myriad functions in cells *in vivo*, for example, protein synthesis gene expression and transcription and translation. Furthermore, presence of binding pockets (much shallow and wide minor groove and narrow major groove pulled deeply into the interior of the molecule) in RNA structure are more suited for ligands involving non-covalent interactions.[24,25] Inorganic metal complexes possess RNA recognition properties as they are (i) coordinatively saturated and inert to substitution (ii) induce RNA strand scission, thus marking their specific binding sites.[26] Few metal complexes have demonstrated to show selectivity and efficiency in targeting non-duplex 3-dimensional RNA.[27,28] Consequently, microRNAs (miRNAs) have emerged as newer metallo-drug therapeutic target for cancers, since the abnormal expression of these noncoding RNAs is associated with the pathogenesis of human cancer.[29,30]

In pursuit of our continuous interest for design of new targeted metal-based antitumor chemotherapeutic agents,[31,32] herein, we report a series of novel tRNA targeted chromone copper-based complexes **1–3** as potent anticancer agents against selected human cancer cell line with GI_{50} < 10 μg mL^{-1} (<20 μM) as determined by SRB assay.

Results and discussion

Synthesis and characterization

The chromone-based copper(II) complexes **1–3** were synthesized and thoroughly characterized by elemental analysis and other spectroscopic techniques *viz.*, UV-vis, FT-IR, EPR and ESI-MS (Scheme 1). The molecular structure of complex **2** was established by single X-ray diffraction studies. The synthesis of complexes involved formation of an *in situ* intermediate (4-

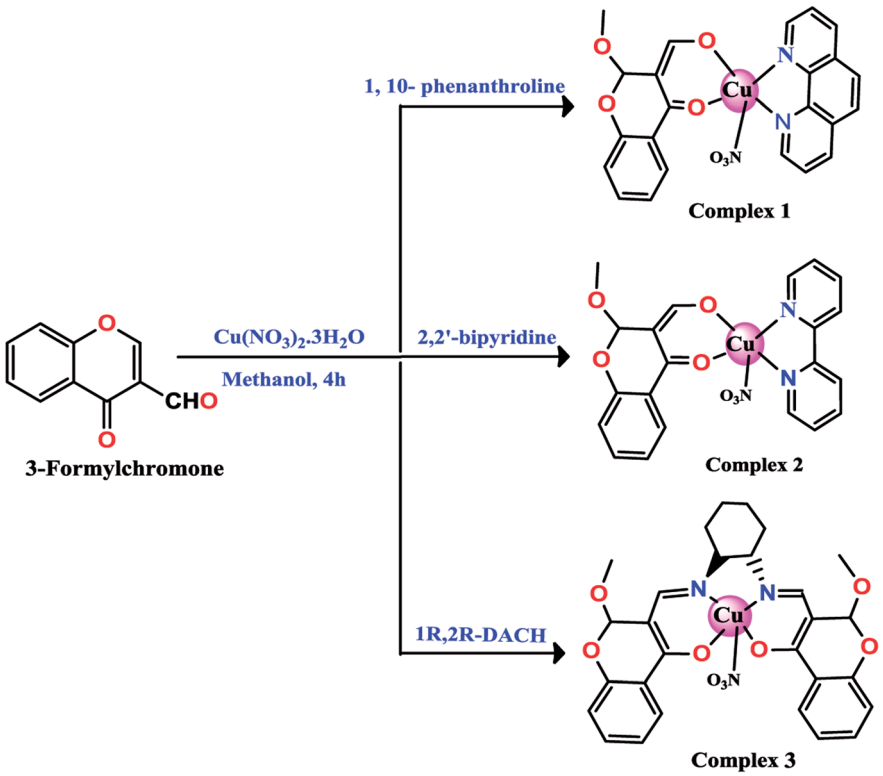

Scheme 1 Synthetic route of complexes **1**, **2** and **3**.

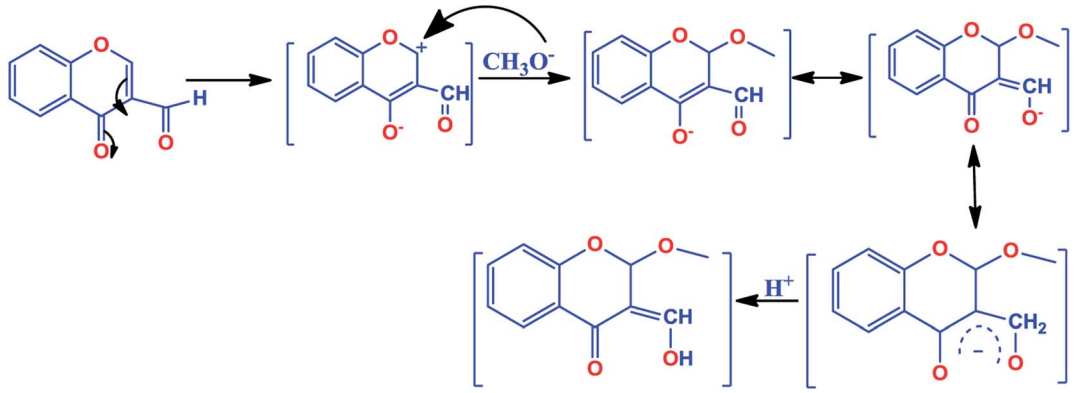

Scheme 2 Mechanism of *in situ* nucleophilic substitution of methoxide anion at 2-position of 3-formylchromone.

hydroxy-2-methoxy-2*H*-chromene-3-carbaldehyde) *via* methoxylation at the 2-position of the chromone ligand (Scheme 2).[13,33] However, complex **3** followed *in situ* formation of azomethine bonds, which was authenticated by characteristic strong band of ν(C=N) at 1607 cm^{-1} in FT-IR and ESI-MS data. All synthesized complexes were found to be stable towards air and soluble in organic solvents, such as MeOH, DCM, DMF and DMSO. The molar conductance values in DMSO for complexes **1–3** revealed their non-electrolytic nature (9.13, 9.61 and 8.17 Ω^{-1} cm^2 mol^{-1}), respectively.

Spectroscopic characterisation

In FT-IR spectra of complexes **1–3**, the characteristic bands assignable to ν(HC=O) and ν(C=O) of 3-formylchromone at 1694 and 1643 cm^{-1} respectively, were shifted to lower wave number indicating possible enolization and their contribution in complex formation (Fig. S1†).[34] IR spectra of complex **3** depicted strong diagnostic band at 1607 cm^{-1} was assigned to ν(C=N) stretching vibration of the coordinated azomethine group.[33,35] Characteristic bands observed at 2972–2900 and 2874–2824 cm^{-1} corresponds to asymmetric and symmetric C–H stretching modes of the CH_3 from methoxy groups ν(Ar–O–CH_3) which confirmed methoxylation of the chromone ligand in complexes.[36] The characteristic band consistent with the asymmetric stretching ($\Delta\nu$ = 58, 79 and 51 cm^{-1} for complexes **1–3**, respectively) in the region 1484–1405 cm^{-1} and in plane bending vibrations ($\Delta\nu$ = 37, 38 and 48 cm^{-1} for complexes **1–3**, respectively) in the region 769–719 cm^{-1} was observed which split into two bands with comparatively small separation, validates unidentate coordination of nitrate ion to the Cu(II) ion in the complexes.[37] In far-IR region, medium intensity signature bands at 500–530 cm^{-1} and 430–410 cm^{-1} were witnessed, attributed to the formation of M–N and M–O vibrations, respectively in all the complexes.[38]

ESI-MS spectra of complexes **1–3** depicted prominent peaks at *m*/*z* 510.80, 486.10 and 613.00 which corresponds to the molecular ion peak $[C_{22}H_{16}CuN_3O_7]^+$, $[C_{20}H_{16}CuN_3O_7]^+$ and $[C_{28}H_{30}CuN_3O_9]^+$, respectively. Other fragmentation peaks for complexes **1–3** were observed at *m*/*z* 448.80, 425.60 and 551.00 which were assigned to $[C_{22}H_{16}CuN_3O_7–NO_3]^+$, $[C_{20}H_{16}CuN_3O_7–NO_3]^+$ and $[C_{28}H_{30}CuN_3O_9–NO_3]^+$ moieties, respectively (Fig. S2†).

Electronic spectra of complexes **1–3** were recorded in DMSO which exhibited two intense absorption bands in the range 252–280 nm and 305–310 nm attributed to π–π^* and n–π^* intraligand transitions, respectively[19] and a lower energy absorption perceived around 350–370 nm was ascribed to LMCT transitions.[39] Weak absorptions corresponding to d–d bands, in the visible region at 640–660 nm validate pentacoordinated geometry around the central Cu(II) center of the complexes.

Paramagnetic nature of the complexes was validated employing EPR in solid state at room temperature on 9.1 GHz frequency under a magnetic field strength of 3000 G (Fig. S3†). X-band EPR spectra of complexes exhibited the isotropic band centered at *g* values given in Table 1. The complexes demonstrated trend $g_{\|} > g_{\perp} > 2.02$, which revealed that the unpaired electron was mainly located in the $d_{x^2-y^2}$ orbital *i.e.* $(eg)^4(a_1g)^2(b_1g)^2(b_2g)^1$, suggesting square pyramidal geometry of copper complexes which is in agreement with the previously reported copper(II) complexes exhibiting similar geometry.[40] Moreover, the complexes possess $g_{\|} < 2.3$ suggesting an appreciable metal–ligand covalent character.

Description of the X-ray crystal structure

Single crystal X-ray diffraction studies revealed that the complex **2** crystallised in triclinic system with space group $P\bar{1}$ possessing lattice parameters, a = 9.2748(7) Å, b = 9.3970(8) Å, c = 12.7651(11) Å, α = 89.293(3), β = 70.077(3) and γ = 72.761(3) per unit cell. An ellipsoid view of complex **2** along with the atom numbering scheme is depicted in Fig. 1(a). Selected bond distances and bond angles are summarized in Table 2. The structure of complex **2** represents an asymmetric Cu(II) ion (CuN_2O_3 coordination environment) coordinated to a chromone ligand moiety through oxygen O,O-atoms with a solvate methoxy group at 2-position, along with two *N*,*N*-donor atoms from heterocyclic 2,2′-bipyridine and a NO_3^- ion. Ligand atoms

Table 1 EPR parameters of complexes **1–3**

Complex	$g_{\|}$	$g_{\perp}$
Complex **1**	2.0940	2.037
Complex **2**	2.0780	2.057
Complex **3**	2.0850	2.048

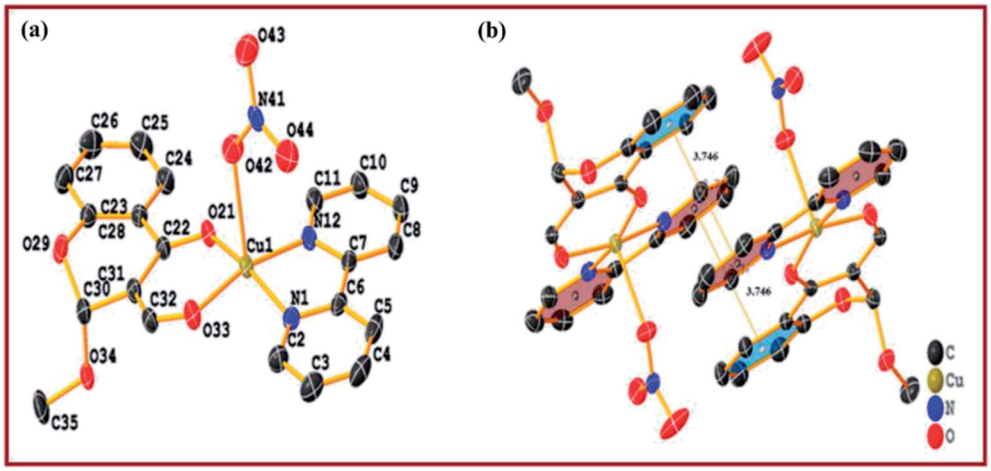

Fig. 1 (a) ORTEP view of complex **2** with partial numbering. Solid thermal ellipsoids are reported at the 50% probability level. (b) Packing diagram of complex **2** showing π–π stacking interaction. Hydrogen atoms have been omitted for clarity.

form square base with oxygen atoms of the chromone carbonyl groups at equatorial positions, *viz.* [Cu(1)–O(33) = 1.9247(12) Å], [Cu(1)–O(21) = 1.9385(11) Å] and nitrogen atoms of 2,2′-bipyridine [Cu(1)–N(1) = 1.9944(14) Å], [Cu(1)–N(12) = 1.9989(14) Å], while nitrate ion makes a long axial coordination [Cu(1)–O(42) = 2.2673(13) Å], which is longer than the equatorial oxygen atoms expected due to presence of two electrons in the d_{z^2} orbital of Cu(II).[38] All Cu–O and Cu–N bond distances observed were within the range of other reported penta-coordinated Cu(II)-based complexes such as $[Cu(nal)(bpy)(H_2O)](ClO_4)$.[38c] Moreover, the structural index value τ of 0.018 [$\tau = (\beta - \alpha)/60$, where α = O(1)–Cu(1)–N(1) = 165.53(9)° and β = O(2)–Cu(1)–N(2) = 170.90(8)°; for perfect square pyramidal and trigonal bipyramidal geometries the τ values are zero and unity, respectively] confirmed slight distorted square pyramidal geometry around copper(II).[41] Packing diagram depicted intermolecular π–π stacking interactions between aromatic rings of 3-formylchromone and 2,2′-bipyridine (Fig. 1(b)). Intermolecular hydrogen bonding interactions [C–O···H, C–H···O and N–O···H] involving methoxy oxygen substituted at 2-position of 3-formylchromone, carbonyl oxygen and distorted nitrato oxygen were observed, facilitating stabilization of complex framework in crystal lattice (Fig. S4†).

Table 2 Selected bond length [Å] and bond angle [deg] of complex **2**

2	
Bond length [Å]	
Cu1–O33	1.9247(12)
Cu1–O21	1.9385(11)
Cu1–N1	1.9944(14)
Cu1–N12	1.9989(14)
Cu1–O42	2.2673(13)
Bond angles [deg]	
O33–Cu1–O21	93.74(5)
O33–Cu1–N1	89.58(5)
O21–Cu1–N12	93.15(5)
N1–Cu1–N12	81.48(6)
O21–Cu1–N1	166.64(5)
O33–Cu1–N12	167.75(5)
O33–Cu1–O42	94.12(5)
O21–Cu1–O42	88.52(5)
N1–Cu1–O42	104.16(5)
N12–Cu1–O42	96.18(5)
C2–N1–C6	119.32(15)
C2–N1–Cu1	125.99(12)
C6–N1–Cu1	114.40(11)

Solution stability studies

The stability of complexes **1–3** has been confirmed using UV-vis spectroscopy by recording absorption spectra in Tris–HCl buffer under physiological conditions (pH = 3.40 & T = 310 K) and at different time intervals (0 h, 2 h, 12 h and 24 h) (Fig. S5†). No change in absorption spectra were recorded in either the intensity or the position of the absorption bands.

Moreover, results did not show any appreciable change in absorption spectra of complexes **1–3** even after 24 h suggesting the stability of complexes under physiological conditions.[42]

Comparative *in vitro* ct-DNA/tRNA binding studies

Electronic absorption titration of complexes **1–3** was evaluated in absence and presence of ct-DNA/tRNA. With cumulative addition of ct-DNA/tRNA (0.00–4.0 × 10^{-5} M) to the fixed concentration of complexes **1–3** (2 × 10^{-4} M), ligand centered LMCT absorption band at 325–400 nm (band I) demonstrated 'hypochromism' (56, 33 and 40%) with a red shift of 2–4 nm, suggestive of intercalation binding mode.[43] Additionally, the band centered at 265–290 nm (band II) exhibited 'hyperchromism' (35, 25 and 30%) accompanied with a blue shift of 5–7 nm indicative of the stabilisation of DNA double helix and RNA.[44] Moreover, complexes **1–3** recorded an isosbestic point at 295–298 nm implicating equilibrium between the free and DNA-bound probe in the ground state indicating only one mode of binding is more dominant with ct-DNA and tRNA (Fig. 2).[45,46] Typically, intercalation involves π-stacking interaction of aromatic chromophore of ligand with nucleic acid base pairs. The observed hypochromism in complexes **1–3** could be

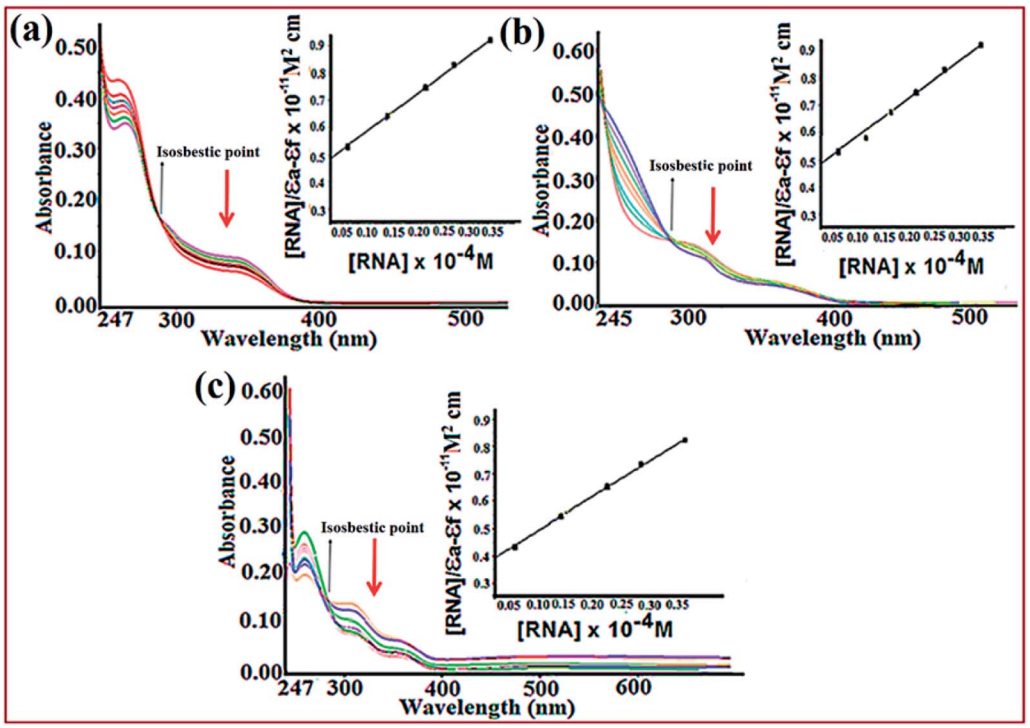

Fig. 2 Absorption spectra of complexes **1** (a), **2** (b) and **3** (c) in absence and presence of increasing concentrations of tRNA in Tris–HCl buffer (pH 7.2). Inset: plots of [RNA]/($\varepsilon_a - \varepsilon_f$) ($M^2$ cm) *vs.* [RNA] for the titration with complexes **1–3**. The arrows specify the intensity change with increasing [tRNA].

attributed to π–π stacking between the aromatic planar chromophore of chromone and *N*,*N*-donor ligand scaffolds with nucleic acid base pairs. To quantitatively compare the binding strengths of complexes **1–3** with ct-DNA/tRNA, the intrinsic binding constant K_b was ascertained, using the Wolfe–Shimer eqn (1):[47]

$$\frac{[\text{DNA or RNA}]}{(\varepsilon_a - \varepsilon_f)} = \frac{[\text{DNA or RNA}]}{(\varepsilon_b - \varepsilon_f)} + \frac{1}{k_b(\varepsilon_b - \varepsilon_f)} \quad (1)$$

where [DNA/RNA] are the ct-DNA/tRNA concentration, and ε_a, ε_f and ε_b are apparent (A_{abs}/[Cu(II) complex]), free and bound complex extinction coefficients, respectively. In a plot of [DNA/RNA]/($\varepsilon_a - \varepsilon_f$) *vs.* [DNA/RNA] with a slope of $1/(\varepsilon_b - \varepsilon_f)$ and intercept of $1/[K_b(\varepsilon_b - \varepsilon_f)]$, K_b values were obtained by the ratio of slope to intercept.

The intrinsic binding constants, K_b values with ct-DNA and tRNA have been calculated which follow the same order for complexes **1** > **3** > **2** but with higher binding propensity for tRNA, greater in magnitude as compared to ct-DNA (Fig. S6†). The observed K_b values are comparable to other reported *N*,*N*-donor copper complexes (Table 3).[48,49] The experimental findings demonstrate stronger interactions of complexes with nucleic acids, specifically targeted to tRNA than ct-DNA which could be due to striking difference in the 3-dimensional morphology of ct-DNA and tRNA. The 'shallow groove side' available in RNA may possibly form hydrogen bonds to the hydroxyl and phosphate groups with the aromatic chromophore ligand *viz.*, chromone and *N*,*N*-donor resulting in higher binding affinity of complexes towards tRNA. Previous literature reports reveal that many small molecules have been designed to target RNAs secondary structure such as bulges and helices.[50] Recently, efforts have been addressed to use many privileged ligand scaffolds (aminoglycosides, macrolides, tetracyclines and oxazolidinones) including metallodrugs to selectively target ncRNAs *viz.*, bacterial RNAs, viral RNAs, and messenger mRNAs but there are fewer reports on Cu(II) based chromone drug entities targeting to RNA.

Table 3 The binding constant values for interaction of complexes **1–3** with ct-DNA/tRNA

			Emission spectroscopy	
Complexes		Absorption spectroscopy K_b ($\times 10^4$ M^{-1})	K ($\times 10^4$ M^{-1})	K_{sv} ($\times 10^4$ M^{-1})
1	ct-DNA	5.81(±0.2)	4.77(±0.31)	6.12(±0.05)
	tRNA	9.4(±0.11)	8.4(±0.1)	9.4(±0.4)
2	ct-DNA	2.5(±0.4)	1.8(±0.08)	3.8(±0.13)
	tRNA	4.7(±0.2)	5.6(±0.05)	7.2(±0.1)
3	ct-DNA	3.05(±0.1)	3.89(±0.4)	4.68(±0.02)
	tRNA	2(±0.12)	6.8(±0.21)	8.8(±0.5)

Binding affinity was improved by introduction of phen moiety in complex **1** which possess planar aromatic ring systems that stacks easily into A–T base pairs by intercalation.[51] Complex **2** showed a relatively less binding affinity which implicates that two non-coplanar pyridyl rings would be engaged in weaker π–π stacking interactions. On the contrary, 1*R*,2*R*-DACH lacks any such planar aromatic ring system, therefore also shows much poor interaction.

Emission spectral titrations of complexes **1–3** with ct-DNA/tRNA was performed to further substantiate the interaction mode. Fluorescence spectra of complexes **1–3** demonstrated an appreciable fluorescence at *ca.* 425–430 nm (λ_{em}) when excited with a wavelength of 305 nm light (λ_{ex}) in absence of ct-DNA/tRNA. With concomitant addition of ct-DNA/tRNA (0–4.00 × 10^{-5} M), a gradual enhancement in the florescence intensity was observed without any apparent shift in emission maxima (Fig. 3). This enhancement in the intensity could be attributed to insertion of complexes into the hydrophobic environment of the interior ct-DNA/tRNA helix, reducing its accessibility to solvent molecules as well as restricting the mobility of complexes at the binding site, which thereby, causes reduction in vibrational modes leading to higher emission intensity.[52]

Binding strength of complexes **1–3** with ct-DNA/tRNA was determined by the binding constant (*K*) value derived from the Scatchard equation[53] which corroborated well with absorption spectral studies (Table 3) which further authenticate our contention that complex **1** strongly bound to tRNA as compared to other complexes and ct-DNA (Fig. S7†).

To further validate the binding mode of complexes, competitive binding studies with ethidium bromide was performed. EB is a strong fluorescent probe for the structure of DNA/RNA and emits fluorescence at *ca.* 600 nm due to strong intercalation between the adjacent base pairs. The enhanced fluorescence intensity was quenched upon addition of the second molecule by replacing the bound EB as the number of binding sites get decreased.[54] With the subsequent addition of complexes **1–3** to EB–ctDNA/EB–tRNA system such that [complex]/[DNA or RNA] = 1 : 1 to 6 : 1, a substantial decrease was observed indicative of competition between EB and complexes towards ct-DNA/tRNA binding attributed to strong intercalation of complexes (Fig. 4). To quantify the magnitude of interaction, quenching efficiency was evaluated using the Stern–Volmer equation.[55] The calculated Stern–Volmer constant, K_{sv} values (Table 3) for **1–3** revealed quenching in the order **1** > **3** > **2**, well corroborated with spectroscopic studies exhibiting strong affinity for tRNA as compared to ct-DNA (Fig. S8†). The binding constant values revealed that complex **1** replaced EB more effectively as compared to complexes **2** and **3**, which is in concordance with the results obtained from UV-vis titration studies.

Circular dichroism

Circular dichroism (CD) is a powerful technique used to monitor the morphological changes during complex–nucleic acids interaction. CD spectra of complexes **1–3** upon incubation with ct-DNA demonstrated a decrease in the intensity of both

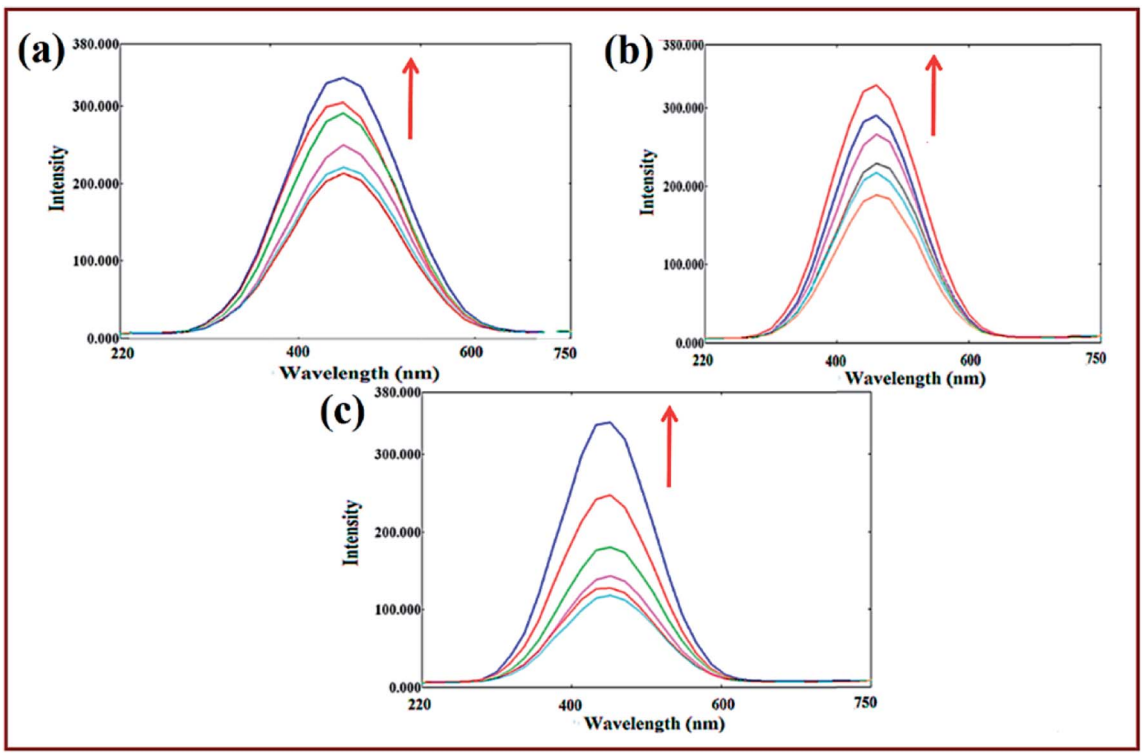

Fig. 3 Emission spectra of complexes **1** (a), **2** (b) and **3** (c) (2×10^{-4} M) in Tris–HCl buffer at pH 7.2 [RNA] = (0–4.00 × 10^{-5} M). Arrows depicts the intensity change upon increasing concentration of tRNA.

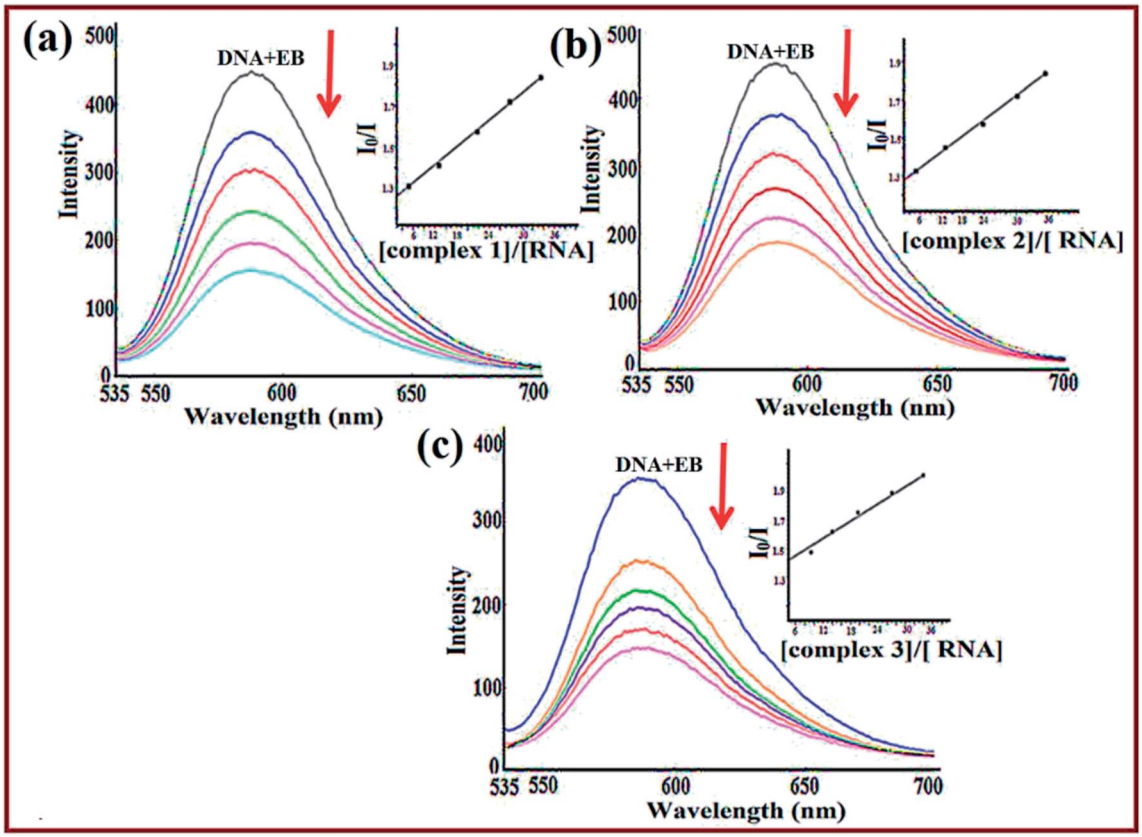

Fig. 4 Emission spectra of EB–tRNA in the absence and presence of complexes **1** (a), **2** (b) and **3** (c) in Tris–HCl buffer at pH 7.2. [Complexes **1–3**] = [EB] = [RNA] = 1.11×10^{-4} M. Arrow indicates change in intensity with increasing concentration of complexes **1–3**.

positive (ellipticity) and negative (helicity) bands with a red shift suggesting intercalation of complexes with ct-DNA (Fig. S9†). The decrease in positive band implicates that complexes could unwind the helix of ct-DNA leading to the loss of helicity. Moreover, red shift observed in the bands revealed that complexes could induce changes in the helicity and base stacking signatures that may result in B → A conformational change of DNA double helix.[56]

The CD spectrum of free tRNA showed four major peaks at 208 and 240 nm (negative), 221 and 270 nm (positive) corresponding to A-conformation of tRNA. With addition of complexes **1–3** ([complex]/[tRNA] = 1), greater amplification in 208 and 270 nm bands was observed whereas the bands at 221 and 240 nm showed decrease to a lesser extent (Fig. S9†).[57] Enhancement in intensity of the band at 270 nm with increase in concentration of complexes **1–3** was in agreement with the intercalative binding mode of complexes with tRNA. Furthermore, absence of any shift in the CD bands at 210 and 270 nm revealed that there was no change in the conformation of tRNA.[58]

EPR spectroscopic studies of complex–ct-DNA/tRNA interactions

EPR spectra of complexes **1–3** were recorded in the absence and presence of (1.4 mg mL^{-1}) ct-DNA/tRNA which exhibited one parallel ($g_{\|}$) and one perpendicular signal ($g_{\perp}$). In presence of ct-DNA/tRNA, EPR spectra of **1** demonstrated weaker signals with slight shift in the $g_{\|}$ value, indicating that complex get bound to ct-DNA/tRNA.[59] However, the spectra of complex–tRNA showed much weaker signals as compared to complex–ct-DNA (Fig. 5). Similarly, complexes **2** and **3** exhibited similar intensity pattern for complex–ct-DNA/tRNA (Fig. S10†).

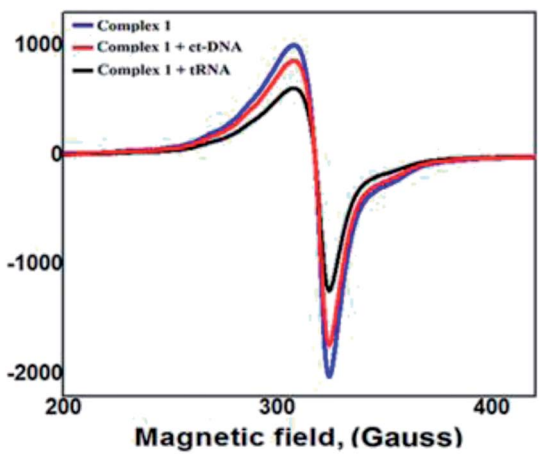

Fig. 5 X-band EPR spectra of 0.3 mM complex **1** (blue), 0.3 mM complex **1** + 1.4 mg mL^{-1} tRNA (black) and 0.3 mM complex **1** + 1.4 mg mL^{-1} ct-DNA (red). Experimental conditions: T = 298 K; microwave frequency = 9.46 GHz; microwave power = 20 mW; 10 G field modulation amplitude; time constant 81.92 ms; conversion time 81.92 ms; 3 accumulations.

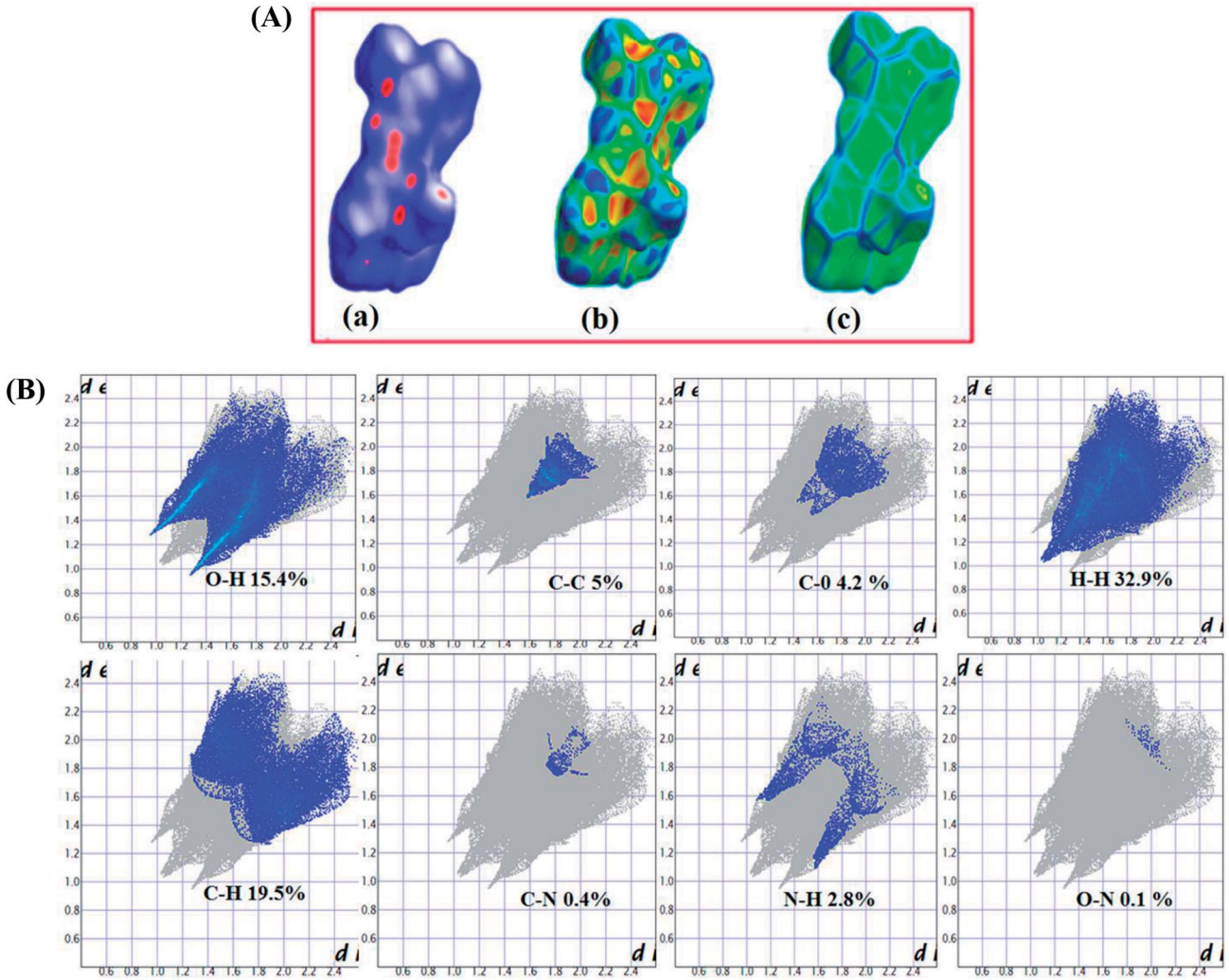

Fig. 6 (A) Hirshfeld surface of complex **2** mapped with d norm (a), shape index (b) and curvedness (c). (B) The 2D fingerprint plots of interatomic interactions of complex **2** showing the percentage of contacts contributed to the total Hirshfeld surface area of the molecules.

Hirshfeld surface analysis

The Hirshfeld surfaces of complex **2** are shown in Fig. 6(A) depicting surfaces that have been mapped over d_{norm} (−0.5 to 1.5 Å), shape index (−1.0 to 1.0 Å) and curvedness (−4.0 to 0.4 Å). The d_{norm} parameter of **2** highlights surface with a red-white-blue coloured scheme where deep red regions correspond to close contact interactions, such as hydrogen bonding contacts *viz.*, C–O···H and N–O···H. White areas depicted contacts around the van der Waals interactions like H···H contacts whereas the blue regions are devoid of such close contacts.[60] The shape index of complex **2** depicted red concave regions with 'bow-tie patterns' which corresponds to C–H···π interactions indicative of the presence of aromatic (π···π) stacking interactions. The curvedness surface represents the electron density present around the different molecular interactions.

The 2D-fingerprint plots of complex **2** provide quantitative information about the contributions arising from various intermolecular interactions to Hirshfeld surfaces (Fig. 6(B)).

Cleavage activity

The DNA cleavage ability of complex **1** was assessed by agarose gel electrophoresis as it exhibited higher binding propensity as compared to other complexes. The gel electrophoretic assay was scrutinized employing supercoiled pBR322 DNA as a substrate in a medium of 5 mM Tris–HCl/50 mM NaCl buffer at pH 7.2. By monitoring the conversion of supercoiled, SC form (Form I) to the nicked circular, NC form (Form II) and linear, LC form (Form III).[61] A concentration-dependent DNA cleavage was performed in order to determine the ability of **1** to cleave SC DNA in the absence of any reducing agent. With increase in concentration of complex **1** (5–30 μM), a more intensified NC, Form II was observed (Fig. 7(a); lane 2–7) demonstrating sufficient conversion of Form I into Form II at 30 μM concentration, implicating efficient single-strand cleavage of the DNA double helix by the complexes.

The cleavage activity of complex **1** was ascertained in presence of exogenous agents *viz.*, ascorbate (Asc), glutathione (GSH), H_2O_2 and 3-mercaptopropionic acid (MPA) which revealed significant enhancement of cleavage pattern which followed the

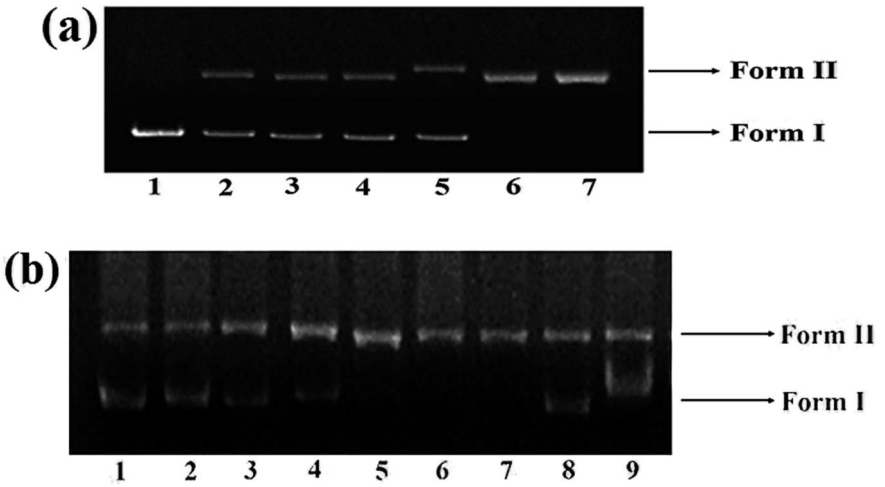

Fig. 7 Agarose gel electrophoretic pattern depicting the cleavage of pBR322 plasmid DNA (300 ng) by complex under different conditions for an incubation time of 45 min at 37 °C. (a) Lane 1, DNA control; lane 2, DNA + **1** (5 μM); lane 3, DNA + **1** (10 μM); lane 4, DNA + **1** (15 μM); lane 5, DNA + 1 (20 μM); lane 6, DNA + **1** (25 μM); lane 7 DNA + **1** (30 μM); (b) lane 1, DNA control, lane 2, DNA + **1** (30 μM) + Asc (0.4 mM), lane 3, DNA + **1** (30 μM) + GSH (0.4 mM), lane 4, DNA + **1** (30 μM) + H_2O_2 (0.4 mM), lane 5, DNA + **1** (30 μM) + MPA (0.4 mM), lane 6, DNA + **1** (30 μM) + DMSO (5 μL); lane 7, DNA + **1** (30 μM) + EtOH (5 μL); lane 8, DNA + **1** (30 μM) + NaN_3 (20 mM); lane 9, DNA + **1** (30 μM) + SOD (5 units).

order H_2O_2 > MPA ≈ GSH > Asc (Fig. 7(b)) similar to cleavage observed for many previously reported copper(II) complexes.[12,62]

Furthermore, to predict the mechanistic pathway of complex **1**, different reactive oxygen species (ROS) *viz.*, EtOH and DMSO (hydroxyl radical scavengers), NaN_3 (singlet oxygen scavenger, $^1O_2$) and SOD (superoxide anion radical, $O_2^{\bullet -}$) were employed to perform DNA cleavage reactions. No significant quenching efficiency of DNA cleavage was observed in presence of DMSO and EtOH (Fig. 7(b)), ruling out the possibility of hydrolytic cleavage pathway, involving diffusible hydroxyl radicals in the cleavage reaction. However, in presence of NaN_3 and SOD, significant inhibition of DNA occurred which implicated oxidative cleavage pathway of complex **1** and suggested that ROS, singlet oxygen quencher, $^1O_2$ and the superoxide anion radical scavenger, $O_2^{\bullet -}$ could be responsible for the cleavage reactions.[63] To predict the hypothesis for DNA cleaving ability of complex **1**, formation of copper peroxide could be perhaps, the suggested mechanistic pathway for oxidative DNA damage of complexes under physiological conditions.[64] In presence of reducing agent *viz.*, H_2O_2, Cu(II) complex **1** may possibly get reduced to Cu(I), which could react with endogenous oxygen to produce hydrogen peroxide, which consequently reacts with another equivalent of Cu(I) complex to generate copper-oxido species with DNA damaging properties. Mostly, cancer cells possess higher intracellular concentration of H_2O_2, which assists the generation of highly active copper-oxido and ROS species which could mediate DNA strand scission *via* oxidative DNA damage the cancerous cells which may induce cell death.[61] DNA cleavage mechanism are given below:

$$\mathrm{Cu(II)} \rightarrow \mathrm{Cu(I)} \quad (2)$$

$$\mathrm{Cu(I)} + \mathrm{O_2} \rightarrow \mathrm{Cu(II)} + \mathrm{O_2^-} \quad (3)$$

$$2\mathrm{O_2^-} + 2\mathrm{H^+} \rightarrow \mathrm{O_2} + \mathrm{H_2O_2} \quad (4)$$

$$\text{ROS species} + \text{DNA} \rightarrow \text{DNA cleavage} \quad (5)$$

The ability of metal ions to promote tRNA cleavage, has the potential to reveal regions of the RNA molecule in close proximity to metal ion on the outer part of the folded RNA molecule. Previous literature reports reveal that single-stranded regions in RNA are spontaneously cleaved 100-fold more effectively than double-stranded regions because single-stranded regions can sample the in-line conformation required for cleavage activity.[65]

In presence of complex **1**, the cleavage pattern of tRNA revealed little effect on tRNA bands after 2 h incubation imitating partial degradation of tRNA. However, pattern of cleavage became more conspicuous on increasing the concentration (6.25–19.37 μM) and with the time of exposure (Fig. 8). The cleavage at a concentration of 19.37 μM was almost complete (80–90%) (Fig. 8; lane 6) and after 6 h, largely diminished intensity band of tRNA was witnessed. Since the cleavage rate enhanced as a function of both incubation time

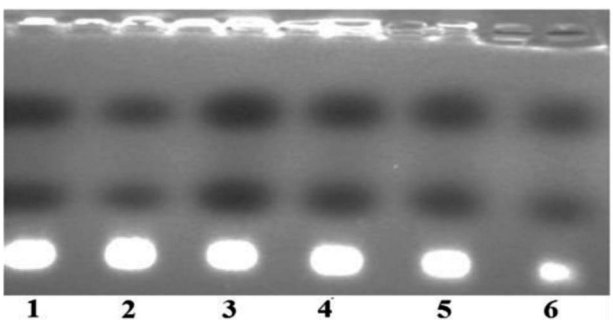

Fig. 8 Agarose gel electrophoretic pattern showing RNA cleavage in buffer after 8 h of incubation time at 37 °C with increasing concentration of complex **1** in a Tris–borate–EDTA (TBE) buffer 40 mM, pH 8.0 buffer, 30 mL of tRNA solution (3×10^{-3} M). Lane 1: tRNA control; lane 2: 6.25 μM of **1** + tRNA; lane 3: 9.25 μM of **1** + tRNA; lane 4: 12.37 μM of **1** + tRNA; lane 5: 15.87 μM of **1** + tRNA; lane 6: 19.37 μM of **1** + tRNA.

and concentration, therefore it was inferred that tRNA cleavage is both time and concentration dependent.

Cytotoxic studies

The cytotoxic activity of complexes **1–3** was investigated against a panel of five human cancer cell lines, *viz.*, MIA-PA-CA-2 (pancreas), HeLa (cervix), A-498 (kidney), MCF-7 (breast) and Hep-G2 (human hepatoma) and was evaluated in terms of GI_{50} values by semi-automated sulforhodamine-B (SRB) assay (Fig. 9). The antitumor screening data revealed excellent anticancer activity complexes **1–3** towards all five cancer cell lines with $GI_{50} < 10$ μg mL^{-1} (<20 μM) values, (Table 4) except complex **2** and complex **3** against MIA-PA-CA-2 and Hep-G2 cell lines, respectively. Interestingly, complex **1** exhibited better anticancer activity towards MIA-Pa-Ca-2, HeLa and MCF-7 cell lines which were even better than that of the standard anticancer drug adriamycin (ADR). The observed results revealed the most potent inhibitory effects of complex **1** against the tested cancer cell lines which corroborated well with the results of binding studies validating the candidature of complex **1** as promising wide spectrum anticancer drug entity. Previous literature reports have also demonstrated remarkable cytotoxicity with significantly lower IC_{50} values of Cu(II) diimine

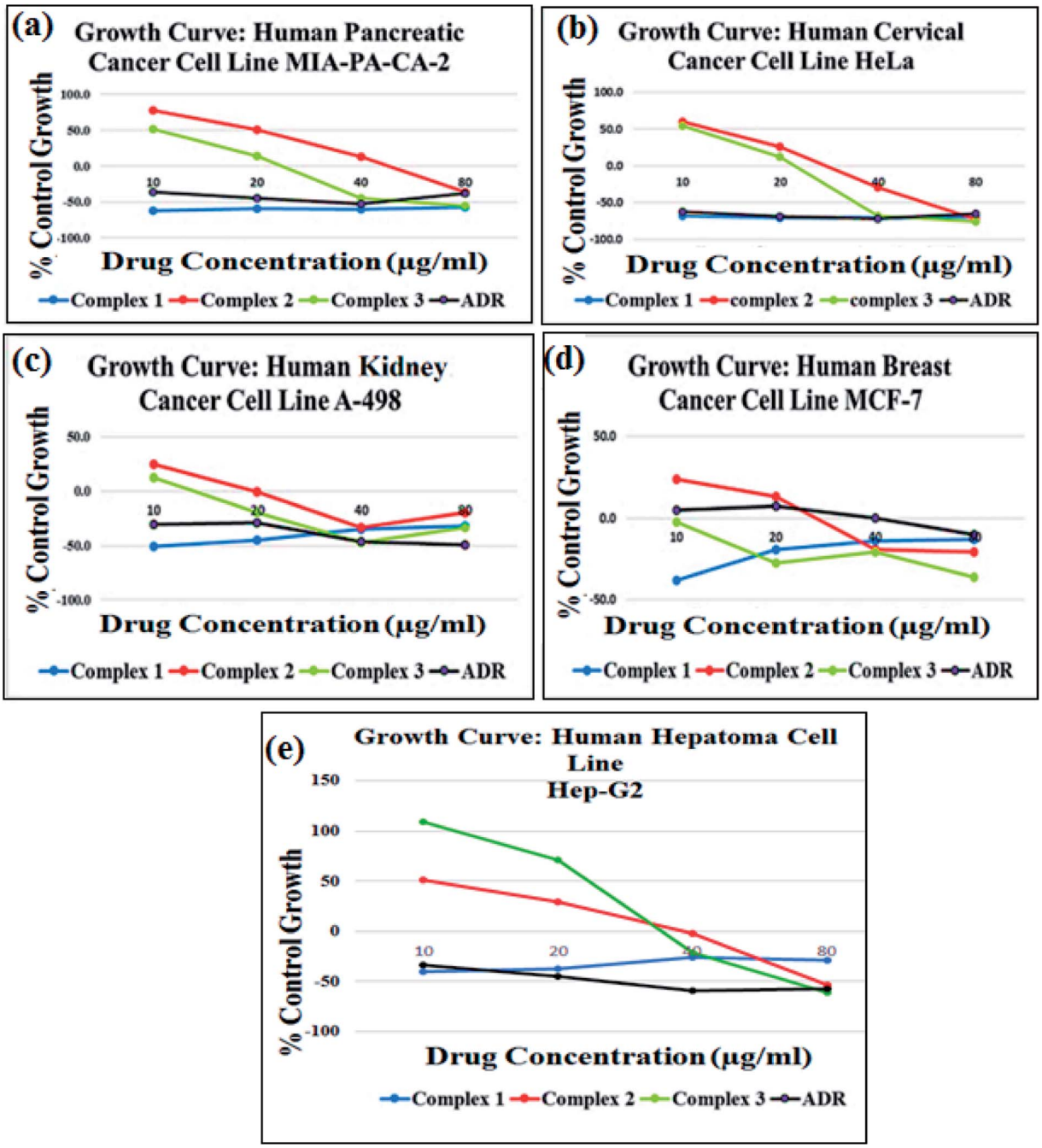

Fig. 9 Growth curve showing % control growth *vs.* drug concentration (μg mL^{-1}) against four different human carcinoma cell lines: (a) MIA-Pa-Ca-2 (pancreas), (b) HeLa (cervix), (c) A-498 (kidney) and (d) MCF-7 (breast) and (e) Hep-G2 (human hepatoma).

Table 4 Summary of the screening data for *in vitro* antitumor activity of complexes **1–3** (in μg mL^{-1})[a]

		Cell lines				
		MIA-PA-CA-2	HeLa	A-498	MCF-7	Hep-G2
GI_{50}	Complex **1**	<10	<10	<10	<10	<10
	Complex **2**	22.3	<10	<10	<10	<10
	Complex **3**	<10	<10	<10	<10	26.9
	ADR	<10	<10	<10	<10	<10
TGI	Complex **1**	NE	<10	<10	NE	<10
	Complex **2**	53.9	35.3	24.4	36.3	41.9
	Complex **3**	31.4	26.6	<10	<10	47.7
	ADR	<10	<10	<10	39.3	<10
LC_{50}	Complex **1**	NE	<10	<10	NE	NE
	Complex **2**	>80	62.6	NE	NE	76.2
	Complex **3**	66.1	54.7	>80	NE	68.5
	ADR	NE	NE	NE	NE	41.9

[a] GI_{50} = growth inhibition of 50% (GI_{50}) calculated from [(Ti − Tz)/(*C* − Tz)]100 = 50, drug concentration that results in a 50% reduction in the net protein increase. ADR = adriamycin (taken as a positive control compound). TGI = tumor growth inhibition. LC_{50} = lethal concentration of 50% (LC_{50}). NE = non-evaluable data.

complexes $[Cu(sal)(diimine)(ClO_4)]_2$ (ref. 38*a*) and [Cu(bimda)(diimine)][38*b*], $[[Cu(nal)(diimine)(H_2O)](ClO_4)]$ against selected cancer cell lines.[38*c*]

The morphological changes observed in MIA-Pa-Ca-2 and MCF-7 cells exposed to complexes **1–3** for a period of 48 h are shown in Fig. 10. Upon exposure of complexes **1–3** to MIA-Pa-Ca-2 and MCF-7 cell lines, a reduction in the normal morphology and cell adhesion capacity was witnessed as compared to the control. Complex **1** exhibited greater selectivity towards the cancer cells which could be attributed to the presence of recognition domain, phen moiety which induces the complex to intercalate into the base pairs of the DNA, consequently, exhibiting better cleavage and cytotoxic properties ultimately, leading to cell death.[66]

Molecular docking studies

Molecular docking studies were employed in order to understand the most probable binding site of complexes **1–3** with ct-DNA. The minor groove of DNA helix acts as a preferred target for small molecules as closer vicinity of strands allows more intimate contact in surface area and therefore, get tightly bind with best fitting.[67] The planarity of ancillary *N*,*N*-donor ligands are compatible for strong π–π stacking interactions of aromatic moieties present in ligands and also for better match of complexes inside ct-DNA strands. The energetically most favorable docked pose revealed that complexes **1–3** interact in the intercalative sites of DNA helix or at the curve contour in narrow and slightly deeper C–G rich region of minor groove of the targeted DNA (Fig. 11(a) and S10†).

Docking studies were also performed with tRNA (PDB ID: 6TNA) to corroborate our spectroscopic results. tRNA consists of well defined 3D structure with regions like D arm, T arm, ψ loop, acceptor stem and anticodon arm which participate directly or indirectly to the target for specific recognition process. The docking results implicated that complexes **1–2** inserted into the active pockets of anticodon arm in close proximity to C-40, A-35, A-36, A-38, G-43, C-40, U-41 and C-28 (Fig. 11(b))[68] whereas **3** was located between upper and lower stem with close proximity to U-59, U-16, U-8, A-21, A-14, C-48, C-63 and G-57 (Fig. S10b†).

The subsequent binding energies of complexes **1–3** calculated for the best-docked pose with ct-DNA target were found to be −289.38, −235.37 and −267 kJ mol^{-1}, respectively and −345.06, −306 and −327 kJ mol^{-1}, respectively for tRNA. More negative binding energy value signifies greater binding propensity of a metal complex, which correlated well with our *in vitro* ct-DNA/tRNA binding.

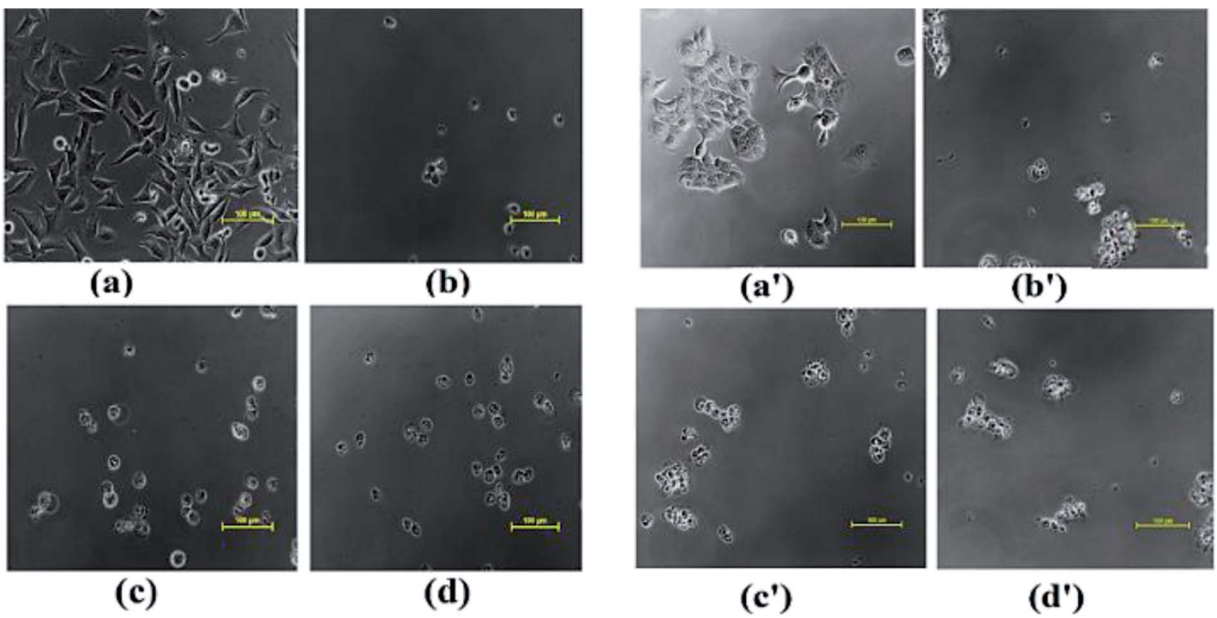

Fig. 10 Morphological changes observed in cancer cell lines on treating with (a) MIA-Pa-Ca-2 control, (b) complexes **1**, (c) **2** and (d) **3**; (a′) MCF-7 control, (b′) complexes, **1** (c′) **2** and (d′) **3**.

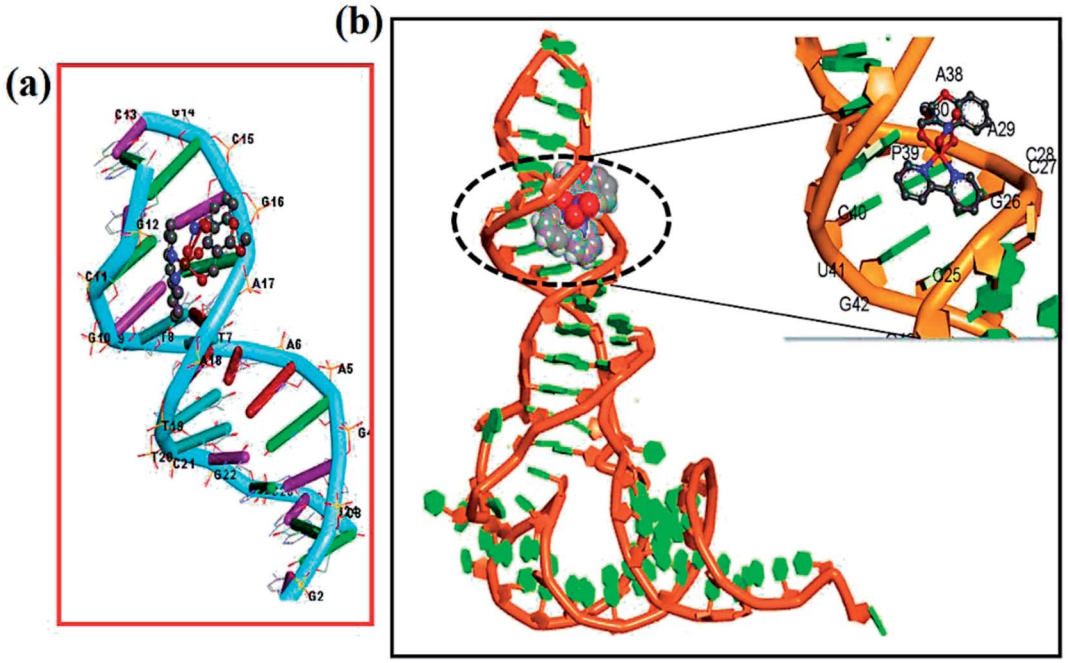

Fig. 11 Molecular docked model of complex **2** with (a) ct-DNA (PDB ID: 1BNA) and (b) tRNA (PDB ID: 6TNA).

Conclusions

New tailored Cu(II) therapeutic entities **1–3** were synthesized from bioactive chromone pharmacophore and *N*,*N*-donor ancillary ligands for their use as antitumor chemotherapeutic agents. The complexes **1–3** were thoroughly characterized by various spectroscopic techniques (IR, UV-vis, EPR and ESI-MS) and single X-ray crystallography in case of complex **2**. Structure activity correlation studies {DNA/RNA binding profile} of complexes **1–3** with ct-DNA/tRNA employing UV-vis, fluorescence, EPR and circular dichroism were carried out. The corroborative results of these experiments showed higher binding propensity of tRNA as compared to ct-DNA. It was observed that by varying the *N*,*N*-donor ligands such as 1,10-phenanthroline, 2,2′-bipyridine and 1*R*,2*R*-DACH (incorporated as recognition domains) in the potential drug molecules, changed the biological activity. For example, complex **1** exhibits structural novelty as it possess an intercalating phen moiety conjugated with 3-formylchromone which showed much pronounced binding with tRNA, higher in the order of magnitude than that of ct-DNA. We also performed the cleavage activity of complexes **1–3** with pBR322 DNA which revealed an efficient single strand cleaving ability in all the complexes; mechanism of cleavage was mediated *via* oxidative pathway involving ROS, singlet oxygen, $^1O_2$ and the superoxide anion, $O_2^{\bullet -}$ and peroxide-assisted cleavage reactions.

Additionally, tRNA cleavage of complexes **1–3** were also employed which revealed efficient cleavage and were both concentration and time dependent. Analysis of Hirshfeld surfaces and fingerprint plots were employed to determine a comparison between intermolecular interactions that involve C–O···H, N–O···H and C–H···O linkages into a two-dimensional framework. In this work, strenuous efforts have been made to design and synthesize successfully tailored tRNA targeted copper-based antitumor drug entities and validated their cytotoxic activity. *In vitro* cytotoxic activity of **1–3** was carried out on a panel of four human cancer cell lines by SRB assay, which revealed that the synthesized complexes were active towards most of the tested cell lines with GI_{50} value < 10 μg mL^{-1} (<20 μM). Moreover, the growth curve data revealed greater potency of complex **1** towards MIA-Pa-Ca-2, HeLa and MCF-7 cell lines which was even better than our standard drug (ADR) and exhibited more potent cytotoxic activity that the other two complexes **2** and **3**. The complex **1** is very promising for chemotherapeutic intervention in pancreatic cancers while the others are active on a wide spectrum of the tested cancer cell lines. Further *in vivo* studies for complex **1** are warranted and are in progress.

Experimental

Materials and instrumentations

3-Formylchromone, 1,10-phenanthroline, 2,2′-bipyridine, 1*R*,2*R*-DACH were purchased from Sigma Aldrich. All reagents were of best commercial grade and were used without any further purification. Molar conductance was measured at room temperature on a Eutech con 510 electronic conductivity bridge. Elemental analysis were employed on Carlo Erba Analyzer Model 1106. Fourier-transform infrared (FT-IR) spectrum were recorded on an Interspec 2020 and Spectrum Two (Perkin Elmer) FT-IR spectrometers. The EPR spectrum of copper complexes **1–3** were assessed on a Varian E 112 ESR spectrometer using X-band frequency (9.5 GHz) at room temperature. ESI-MS spectra were recorded on Micromass Quattro II triple

quadrupole mass spectrometer. Electronic and emission spectrum were recorded on UV-1700 PharmaSpec UV-vis spectrophotometer (Shimadzu) and RF-5301PC Spectrofluorophotometer (Shimadzu), respectively. CD spectra were obtained on Jasco J-815-CD spectropolarimeter. All experiments involving the interaction of complexes **1–3** with ct-DNA/tRNA were carried out in aerated buffer (5 mM Tris–HCl, 50 mM NaCl, pH = 7.2). The concentration per base pairs for both ct-DNA and tRNA were obtained spectrophotometrically by assuming ε_{260} nm values to be 6600 and 7700 M^{-1} cm^{-1}, respectively.[69] Cleavage experiments were performed with the help of Axygen electrophoresis supported by a Genei power supply with a potential range of 50–500 V, visualized and photographed by a Vilber-INFINITY gel documentation system.

Synthesis of Cu(II) complexes

Synthesis of [Cu(L)(phen)(NO_3)] (1). Complex **1** was synthesized by mixing methanolic solutions of 3-formylchromone (L) (0.174 g, 1 mmol), copper(II) nitrate trihydrate (0.295 g, 1 mmol) and 1,10-phenanthroline (0.181 g, 1 mmol) in 1 : 1 : 1 stoichiometric ratio under reflux condition for 4 h. The resulting solution was filtered and kept aside for slow evaporation at room temperature. Green precipitate was collected after 3 days which were soluble in organic solvents like MeOH, DCM, DMF and DMSO.

Yield: 84%, melting point: 195 °C. Elemental analysis calculated for $C_{22}H_{16}CuN_3O_7$: C, 54.07; H, 3.35; N, 8.22. Found: C, 54.87; H, 3.40; N, 8.12. FT-IR (KBr, υ_{max}/cm^{-1}): 3237 ν(C–H), 1617.01 ν(C=O), 2955.92 $\nu_{asym}(OCH_3)$, 2874.89 $\nu_{sym}(OCH_3)$, 1484, 1426 $\nu_{asym}(NO_3)$, 757, 720 $\nu_{bend}(NO_3)$. UV-vis (1×10^{-3} M, DMSO, λ_{max}, nm) 285, 305, 365 and 652 ($\varepsilon = 225$ M^{-1} cm^{-1}) (d–d transition). Λ_M (1×10^{-3} M, DMSO): 9.13 Ω^{-1} cm^2 mol^{-1} (non-electrolyte). ESI-MS (CH_3OH): found m/z = 448.80 $[Cu(L)(phen)]^+$ (calcd m/z = 448.05).

Synthesis of [Cu(L)(bpy)(NO_3)] (2). Complex **2** was synthesized by reacting methanolic solution of 3-formylchromone (0.174 g, 1 mmol), copper(II) nitrate trihydrate (0.295 g, 1 mmol) and 2,2′-bipyridine (0.156 g, 1 mmol) in the molar ratio 1 : 1 : 1 under reflux condition for 4 h. The resulting solution was filtered and allowed to evaporate slowly at room temperature. Blue crystals suitable for single X-ray crystallography were obtained after 3–4 days of slow evaporation of the reaction mixture which were found to be stable towards air and soluble in organic solvents like MeOH, DCM, DMF and DMSO.

Yield: 80%, melting point: 185 °C. CCDC no. 1574863. Elemental analysis calculated for $C_{20}H_{16}CuN_3O_7$: calc. C, 51.80; H, 3.52, N, 8.63. Found: C, 51.01; H, 3.34, N, 8.96. FT–IR (KBr, υ_{max}/cm^{-1}): 2918 ν(C–H), 1619.7 ν(C=O), 2927.29 $\nu_{asym}(OCH_3)$ and 2874.48 $\nu_{sym}(OCH_3)$, 1484, 1405 $\nu_{asym}(NO_3)$, 769, 731 $\nu_{bend}(NO_3)$. UV-vis (1×10^{-3} M, DMSO, λ_{max}, nm): 293, 306, 362 and 660 ($\varepsilon = 200$ M^{-1} cm^{-1}) (d–d transition). Λ_M (1×10^{-3} M, DMSO): 9.61 Ω^{-1} cm^2 mol^{-1} (non-electrolyte). ESI-MS (CH_3OH): found m/z = 425.60 $[Cu(L)(bpy)]^+$ (calcd m/z = 424.05).

Synthesis of [Cu(L)(DACH)(NO_3)] (3). Complex **3** was synthesized by reacting methanolic solutions of 3-formylchromone (0.348 g, 2 mmol), copper(II) nitrate trihydrate (0.295 g, 1 mmol) and 1*R*,2*R*-DACH (0.114 g, 1 mmol) in molar ratio 2 : 1 : 1 under reflux for 4 h. The resulting solution was filtered. Very fine green coloured needle like crystals were obtained upon slow evaporation of solvent at room temperature.

Yield: 70%, melting point: 180 °C. Elemental analysis calculated for $C_{28}H_{30}CuN_3O_9$: C, 54.76; H, 4.60; N, 6.84; found C, 54.82; H, 4.77; N, 6.71. FT-IR (KBr, υ_{max}/cm^{-1}): 3278 ν(N–H), 1607.00 ν(HC=N), 1666.19 ν(C=O), 2936.36 $\nu_{asym}(OCH_3)$, 2860.87 $\nu_{sym}(OCH_3)$, 1481, 1433 $\nu_{asym}(NO_3)$, 767, 719 $\nu_{bend}(NO_3)$. UV-vis (1×10^{-3} M, DMSO, λ_{max}, nm): 237, 260, 310, 362 and 645 ($\varepsilon = 110$ M^{-1} cm^{-1}) (d–d transition). Λ_M (1×10^{-3} M, DMSO): 8.17 Ω^{-1} cm^2 mol^{-1} (non-electrolyte). ESI-MS (CH_3OH): found m/z = 551.00 $[Cu(L)(DACH)]^+$ (calcd m/z = 551.12).

Description of X-ray crystal structure

Single crystal X-ray structural studies of complex **2** was performed on a D8 VENTURE Bruker AXS diffractometer [*], employing graphite-mono-chromated Mo-Kα radiation generated from a fine-focus sealed tube ($\lambda = 0.71073$ Å) at 150 K. The structure was solved by dual-space algorithm using the SHELXT program[70] and further refined with full-matrix least-square methods based on F2 (SHELXL).[71] All non-hydrogen atoms were refined with anisotropic atomic displacement parameters. H atoms were finally included in their calculated position. The drawing of the complex was realized with PLATON.[72] A summary of selected crystallographic information for complex **2** is given in Table 5.

In vitro binding and cleavage experiments

Nucleic acids (ct-DNA/tRNA) binding experiments were carried out in Tris–HCl/NaCl (5 : 50 mM) buffer at pH 7.2 by employing

Table 5 Crystallographic data for complex **2**

Parameters	**2**
CCDC no.	1574863
Formula	$C_{21}H_{17}CuN_3O_7$
Fw (g mol^{-1})	486.92
Crystal system	Triclinic
Space group	$P\bar{1}$
a (Å)	9.2748(7)
b (Å)	9.3970(8)
c (Å)	12.7651(11)
α (deg)	89.293(3)
β (deg)	70.077(3)
γ (deg)	72.761(3)
U (Å^3)	994.09(14)
Z	2
ρ_{calc} (g cm^{-3})	1.627
(mm^{-1})	1.150
F (000)	498.0
Crystal size (mm)	0.150 × 0.060 × 0.020
Temp (K)	150 K
Measured reflns	23 356
GOF[a]	1.055
R^b [$I > 2\sigma(I)$]	0.0254
w$R_2{}^b$ (all data)	0.0679

[a] GOF is defined as $\{\Sigma[w(F_0{}^2 - F_c{}^2)]/(n-P)\}^2$ where n is the number of data and p is the number of parameters. [b] $R = \{\Sigma||F_0| - |F_c||/\Sigma|F_0|\}$, w$R^2 = \{\Sigma w(F_0{}^2 - F_c{}^2)^2/\Sigma w(F_0{}^2)^2\}^{1/2}$.

absorption spectroscopy, emission spectroscopy and circular dichroism following previously used standard methods and practices espoused by our laboratory.[73] The cleavage experiments of complex **1** using supercoiled pBR322 DNA (300 ng) in Tris–HCl/NaCl (5 : 50 mM) buffer at pH 7.2 were performed using agarose gel electrophoresis. Furthermore, tRNA cleavage experiments were performed in a Tris–HCl 40 mM, pH 8.0 buffer by incubating the reaction mixture containing increasing concentration of complexes **1–3** for 24 h at 37 °C. The gel electrophoresis assay was carried out in presence of Tris–borate–EDTA buffer (TBE) for 180 min at 50 V cm^{-1}. The gel was then allowed soaked for 30 min in and rinsed with distilled water. RNA fragments was further visualized, after incubation with EB (0.6 mg mL^{-1}), using an UV transilluminator.

Hirshfeld surface analysis

Hirshfeld analysis along with 2D fingerprint plot for complex **2** was generated using crystal Explorer 3.1 (ref. 74) software based on results of single crystal X-ray diffraction studies.

Molecular docking studies

Molecular docking studies were assessed using HEX 8.0 software.[75] The structures of complexes **1–3** were converted into PDB format prior performing docking experiments. The crystal structures of ct-DNA (PDB ID: BDNA) and tRNA (PDB ID: 6TNA) were downloaded from protein data bank (http://www.rcsb.org./pdb). Visualization of complexes **1–3** has been done by Discovery Studio molecular graphics program.

Cytotoxic studies

In vitro antitumor screening of **1–3** was performed on human cancer lines of four different histological origin *viz.*, MIA-PA-CA-2 (pancreas), HeLa (cervix), A-498 (kidney) and MCF-7 (breast). The cell lines used in the experiment were obtained from NCI, USA and NCCS, Pune. Human malignant cell lines were grown and obtained in RPMI-1640 medium supplemented with 10% Fetal Bovine Serum (FBS) and antibiotics to study the growth pattern of these cells. The cells proliferation upon treatment with chemotherapy was determined by means of SRB assay.[76]

Conflicts of interest

There are no conflicts to declare.

Abbreviations

phen	1,10-Phenanthroline
Bpy	2,2′-Bipyridine
ct-DNA	Calf thymus DNA
1*R*,2*R*-DACH	1*R*,2*R*-Diaminocyclohexane
tRNA	Yeast transfer RNA
SRB	Sulforhodamine-B
ADR	Adriamycin

Acknowledgements

The authors are thankful to SAIF, CIL, Panjab University, Chandigarh, for ESI-MS and elemental analysis facility. The authors are grateful to ACTREC, Mumbai for carrying out the cytotoxic studies. Financial support to the Department of Chemistry, Aligarh Muslim University from the UGC under SAP DRS II Scheme and the DST under PURSE phase II programme is gratefully acknowledged. The author (Z. Afsan) expresses her gratitude to DST for fellowship under PURSE phase II programme.

References

1 (*a*) V. Gandin, F. Tisato, A. Dolmella, M. Pellei, C. Santini, M. Giorgetti, C. Marzano and M. Porchia, *J. Med. Chem.*, 2014, **57**, 4745–4760; (*b*) Y. Gou, J. Qi, J. P. Ajayi, Y. Zhang, Z. Zhou, X. Wu, F. Yang and H. Liang, *Mol. Pharmaceutics*, 2015, **12**, 3597–3609.

2 T. Hofbeck, U. Monkowius and H. Yersin, *J. Am. Chem. Soc.*, 2015, **137**, 99–404.

3 (*a*) C. Chen, X. H. Xu, B. Yang and F. L. Qing, *Org. Lett.*, 2014, **16**, 3372–3375; (*b*) B. Kumar Ghosh, S. Hazra, B. Naik and N. N. Ghosh, *Powder Technol.*, 2015, **269**, 371–378.

4 D. Denoyer, S. Masaldan, S. L. Fontaine and M. A. Cater, *Metallomics*, 2015, **7**, 1459–1476.

5 L. R. Azuara and M. E. B. Gómez, *Curr. Med. Chem.*, 2010, **17**, 3606–3615.

6 L. Finney, S. Vogt, T. Fukai and D. Glesne, *Clin. Exp. Pharmacol. Physiol.*, 2009, **36**, 88–94.

7 M. M. Eatock, A. Schatzlein and S. B. Kaye, *Cancer Treat. Rev.*, 2000, **26**, 191–204.

8 M. Grazul and E. Budzisz, *Coord. Chem. Rev.*, 2009, **253**, 2588–2598.

9 J. Reis, A. Gaspar, N. Milhazes and F. Borges, *J. Med. Chem.*, 2017, **60**, 7941–7957.

10 A. Gaspar, M. J. Matos, J. Garrido, E. Uriarte and F. Borges, *Chem. Rev.*, 2014, **114**, 4960–4992.

11 R. S. Keri, S. Budagumpi, R. K. Pai and R. G. Balakrishna, *Eur. J. Med. Chem.*, 2014, **78**, 340–374.

12 M. Usman, M. Zaki, R. A. Khan, A. Alsalme, M. Ahmad and S. Tabassum, *RSC Adv.*, 2017, **7**, 36056–36071.

13 I. Yousuf, F. Arjmand, S. Tabassum, L. Toupet, R. A. Khan and M. A. Siddiqui, *Dalton Trans.*, 2015, **44**, 10330–10342.

14 (*a*) M. Andrs, J. Korabecny, D. Jun, Z. Hodny, J. Bartek and K. Kuca, *J. Med. Chem.*, 2015, **58**, 41–71; (*b*) S. Singh, A. T. Baviskar, V. Jain, N. Mishra, U. C. Banerjee, P. V. Bharatam, K. Tikoo and M. P. S. Isha, *MedChemComm*, 2013, **4**, 1257–1266.

15 R. H. Erickson, K. J. Natalie, W. Bock, Z. Lu, F. Farzin, R. G. Sherrill, D. J. Meloni, R. J. Sherrill, D. J. Meloni, R. J. Patch, W. J. Rzesotarski, J. Clifton, M. J. Pontecorvo, M. A. Bailey, K. Naper and W. Karbon, *J. Med. Chem.*, 1992, **35**, 1526–1535.

16 G. Kalaiarasi, S. R. J. Rajkumar, S. Dharani, V. M. Lynch and R. Prabhakaran, *Inorg. Chim. Acta*, 2018, **471**, 759–776.

17 B. D. Wang, Z. Y. Yang, M. H. Lü, J. Hai, Q. Wang and Z. N. Chen, *J. Organomet. Chem.*, 2009, **694**, 4069–4075.
18 V. Barve, F. Ahmed, S. Adsule, S. Banerjee, S. Kulkarni, P. Katiyar, C. E. Anson, A. K. Powell, S. Padhye and F. H. Sarkar, *J. Med. Chem.*, 2006, **49**, 3800–3808.
19 M. Gaber, N. El-Wakiel, K. El-Baradie and S. Hafez, *J. Iran. Chem. Soc.*, 2018, DOI: 10.1007/s13738-018-1494-9.
20 I. Correia, S. Borovic, I. Cavaco, C. P. Matos, S. Roy, H. M. Santose, L. Fernandese, J. L. Capeloe, L. R. Azuarag and J. C. Pessoa, *J. Inorg. Biochem.*, 2017, **175**, 284–297.
21 (*a*) L. Gasque, R. M. Esparza and L. R. Ramirez, *J. Inorg. Biochem.*, 1992, **48**, 121–127; (*b*) W. L. Kwik and K. P. Ang, *J. Inorg. Nucl. Chem.*, 1980, **42**, 303–313.
22 E. Wong and C. M. Giandomenico, *Chem. Rev.*, 1999, **99**, 2451–2466.
23 G. Gasser, I. Ott and N. M. Nolte, *J. Med. Chem.*, 2011, **54**, 3–25.
24 S. Stern, B. Weiser and H. F. Noller, *J. Mol. Biol.*, 1988, **204**, 447–481.
25 L. Guan and M. D. Disney, *ACS Chem. Biol.*, 2012, **7**, 73–86.
26 C. S. Chow and F. M. Bogdan, *Chem. Rev.*, 1997, **97**, 1489–1513.
27 H. Xu, Y. Liang, P. Zhang, F. Du, B. R. Zhou, J. Wu, J. H. Liu, Z. G. Liu and L. N. Ji, *J. Biol. Inorg Chem.*, 2005, **10**, 529–538.
28 M. Cusumano, M. Letizia, D. Pietro, A. Giannetto and P. A. Vainiglia, *Inorg. Chem.*, 2007, **46**, 7148–7153.
29 K. Kota and S. Balasubramanian, *Drug Discovery Today*, 2010, **15**, 733–740.
30 D. M. Pereira, P. M. Rodrigues, P. M. Borralho and C. M. P. Rodrigues, *Drug Discovery Today*, 2013, **18**, 282–288.
31 M. Chauhan, K. Banerjee and F. Arjmand, *Inorg. Chem.*, 2007, **46**, 3072–3082.
32 R. A. Khan, S. Yadav, Z. Hussain, F. Arjmand and S. Tabassum, *Dalton Trans.*, 2014, **43**, 2534–2548.
33 T. Rosu, E. Pahontu, C. Maxim, R. Georgescu, N. Stanica, G. L. Almajan and A. Gulea, *Polyhedron*, 2010, **29**, 757–766.
34 M. Shebl, O. M. I. Adly, A. Taha and N. N. Elabd, *J. Mol. Struct.*, 2017, **1147**, 438–451.
35 (*a*) K. Nakamoto, *Infrared Spectra of Inorganic and Coordination Compounds*, Wiley and Sons, New York, 1986, pp. 212, 232, 248, 251 and 256; (*b*) K. Nakamoto, *Infrared and Raman Spectra of Inorganic and Coordination Compounds*, Wiley-Interscience, New York, 5th edn, 1997, p. 86.
36 A. D. Kulaczkowska and L. Mazur, *J. Mol. Struct.*, 2011, **985**, 233–242.
37 (*a*) A. S. Potapov, E. A. Nudnov, A. I. Khlebnikov, V. D. Ogorodnikov and T. V. Petrenko, *Inorg. Chem. Commun.*, 2015, **53**, 72–75; (*b*) B. Gliši, I. Aleksic, P. Comba, H. Wadepohl, T. Ilic-Tomic, J. Nikodinovic-Runic and M. I. Djuran, *RSC Adv.*, 2016, **6**, 86695–86709; (*c*) G. Sridhar, I. Mohammed Bilal, D. Easwaramoorthy, S. Kutti Rani, B. S. Kumar and C. Sai Manohar, *J. Braz. Chem. Soc.*, 2017, **28**, 756–767.
38 (*a*) R. Loganathan, S. Ramakrishnan, E. Suresh, M. Palaniandavar, A. Riyasdeend and M. A. Akbarsha, *Dalton Trans.*, 2014, **43**, 6177–6194; (*b*) R. Loganathan, S. Ramakrishnan, M. Ganeshpandian, N. S. P. Bhuvanesh, M. Palaniandavar, A. Riyasdeend and M. A. Akbarsha, *Dalton Trans.*, 2015, **44**, 10210–10227; (*c*) R. Loganathan, M. Ganeshpandian, N. S. P. Bhuvanesh, M. Palaniandavara, A. Muruganantham, S. K. Ghosh, A. Riyasdeen and M. A. Akbarsha, *J. Inorg. Biochem.*, 2017, **174**, 1–13.
39 M. Alagesan, P. Sathyadevi, P. Krishnamoorthy, N. S. P. Bhuvanesh and N. Dharmaraj, *Dalton Trans.*, 2014, **43**, 15829–15840.
40 (*a*) U. M. Rafi, D. Mahendiran, A. K. Haleel, R. P. Nankar, M. Doble and A. K. Rahiman, *New J. Chem.*, 2016, **40**, 2451–2465; (*b*) N. Joksimović, D. Baskić, S. Popović, M. Zarić, M. Kosanić, B. Ranković, T. Stanojković, S. B. Novaković, G. Davidović, Z. Bugarčića and N. Janković, *Dalton Trans.*, 2016, **45**, 15067–15077.
41 (*a*) G. Murphy, P. Nagle, B. Murphy and B. Hathway, *Dalton Trans.*, 1997, 2645–2652; (*b*) P. T. Selvi, M. Murali, M. Palaniandavar, M. Kockerling and G. Henkel, *Inorg. Chim. Acta*, 2002, **340**, 139–146.
42 M. Muralisankar, J. Haribabu, N. S. P. Bhuvanesh, R. Karvembu and A. Sreekanth, *Inorg. Chim. Acta*, 2016, **449**, 82–95.
43 T. M. Kelly, A. B. Tossi, D. J. McConnell and T. C. Strekas, *Nucleic Acids Res.*, 1985, **13**, 6017–6034.
44 (*a*) C. Tolia, A. N. Papadopoulos, C. P. Raptopoulou, V. Psycharis, C. Garino, L. Salassa and G. Psomas, *Eur. J. Med. Chem.*, 2013, **123**, 53–65; (*b*) N. Biswas, S. Khanra, A. Sarkar, S. Bhattacharjee, D. Prasad Mandal, A. Chaudhuri, S. Chakraborty and C. R. Choudhury, *New J. Chem.*, 2017, **41**, 12996–13011.
45 K. W. Kohn, M. J. Waring, D. Glaubiger and C. A. Friedman, *Cancer Res.*, 1975, **35**, 71–76.
46 M. Nath, M. Vats and P. Roy, *Chem. Sustainable Dev.*, 2012, 301–315.
47 A. Wolfe, G. H. Shimer Jr and T. Meehan, *Biochemistry*, 1987, **26**, 6392–6396.
48 S. S. Bhat, A. A. Kumbhar, H. Heptullah, A. A. Khan, V. V. Gobre, S. P. Gejji and V. G. Puranik, *Inorg. Chem.*, 2011, **50**, 545–558.
49 Z. Chen, M. Tan, L. Liu, Y. Liu, H. Wang, B. Yang, A. Peng, H. Liu, H. Liang and C. Orvig, *Dalton Trans.*, 2009, **48**, 10824–10833.
50 X. Liang, X. Zou, L. Tan and W. Zhu, *J. Inorg. Biochem.*, 2010, **104**, 1259–1266.
51 (*a*) S. Kathiresan, S. Mugesh, M. Murugan, F. Ahamed and J. Annaraj, *RSC Adv.*, 2016, **6**, 1810–1825; (*b*) J. G. Liu, Q. L. Zhang and L. N. Ji, *Transition Met. Chem.*, 2001, **26**, 733–738.
52 (*a*) L. F. Tan, H. Chao, K. C. Zhen, J. J. Fei, F. Wang, Y. F. Zhou and L. N. Ji, *Polyhedron*, 2007, **26**, 5458–5468; (*b*) K. A. Meadows, F. Liu, J. Sou, B. P. Hudson and D. R. McMillin, *Inorg. Chem.*, 1993, **32**, 2919–2923.
53 E. F. Healy, *J. Chem. Educ.*, 2007, **84**, 1304–1307.
54 J. B. LePecq and C. Paoletti, *J. Mol. Biol.*, 1967, **27**, 87–106.
55 K. S. Ghosh, B. K. Sahoo, D. Jana and S. Dasgupta, *J. Inorg. Biochem.*, 2008, **102**, 1711–1718.

56 (*a*) P. U. Maheswari and M. Palaniandavar, *J. Inorg. Biochem.*, 2004, **98**, 219–230; (*b*) F. Bisceglie, S. Pinelli, R. Alinovi, M. Goldoni, A. Mutt, A. Camerini, L. Piola, P. Tarasconi and G. Pelosi, *J. Inorg. Biochem.*, 2014, **140**, 111–125.

57 (*a*) S. K. Seth, D. Sarkar, A. D. Jana and T. Kar, *Cryst. Growth Des.*, 2011, **11**, 4837–4849; (*b*) M. Mitra, S. K. Seth, S. R. Choudhury, P. Manna, A. Das, M. Helliwell, A. Bauza, A. Frontera and S. Mukhopadhyay, *Eur. J. Inorg. Chem.*, 2013, 4679–4685; (*c*) S. K. Seth, *Inorg. Chem. Commun.*, 2014, **43**, 60–63.

58 (*a*) X. Qiao, Z. Y. Ma, J. Shao, W. G. Bao, J. Y. Xu, Z. Y. Qiang and J. S. Lou, *BioMetals*, 2014, **27**, 155–172; (*b*) G. Y. Li, K. J. Du, J. Q. Wang, J. W. Liang, J. F. Kou, X. J. Hou, L. N. Ji and H. Chao, *J. Inorg. Biochem.*, 2013, **119**, 43–53.

59 (*a*) A. Draksharapu, A. J. Boersma, M. Leising, A. Meetsma, W. R. Browne and G. Roelfes, *Dalton Trans.*, 2015, **44**, 3647–3655; (*b*) T. E. Edwards, T. M. Okonogi and S. T. Sigurdsson, *Chem. Biol.*, 2002, **9**, 699–706; (*c*) A. Raja, V. Rajendiran, P. U. Maheswari, R. Balamurugan, C. A. Kilner, M. A. Halcrow and M. Palaniandavar, *J. Inorg. Biochem.*, 2005, **99**, 1717–1732.

60 A. Mazumder, C. L. Sutton and D. S. Sigman, *Inorg. Chem.*, 1993, **32**, 3516–3520.

61 V. A. Kawade, A. A. Kumbhar, A. S. Kumbhar, C. Nather, A. Erxleben, U. B. Sonawane and R. R. Joshi, *Dalton Trans.*, 2011, **40**, 639–650.

62 W. J. Lian, X. T. Wang, C. Z. Xie, H. Tian, X. Q. Song, H. T. Pan, X. Qiao and J. Y. Xu, *Dalton Trans.*, 2016, **45**, 9073–9087.

63 (*a*) G. Y. Li, K. J. Du, J. Q. Wang, J. W. Liang, J. F. Kou, X. J. Hou, L. N. Ji and H. Chao, *J. Inorg. Biochem.*, 2013, **119**, 43–53; (*b*) D. D. Li, J. L. Tian, W. Gu, X. Liu, H. H. Zeng and S. P. Yan, *J. Inorg. Biochem.*, 2011, **105**, 894–901; (*c*) M. Forconi and D. Herschlag, *Methods Enzymol.*, 2009, **468**, 91–106.

64 F. Arjmand, I. Yousuf, T. B. Hadda and L. Toupet, *Eur. J. Med. Chem.*, 2014, **81**, 76–88.

65 (*a*) G. Y. Li, K. J. Du, J. Q. Wang, J. W. Liang, J. F. Kou, X. J. Hou, L. N. Ji and H. Chao, *J. Inorg. Biochem.*, 2013, **119**, 43–53; (*b*) D. D. Li, J. L. Tian, W. Gu, X. Liu, H. H. Zeng and S. P. Yan, *J. Inorg. Biochem.*, 2011, **105**, 894–901; (*c*) M. Forconi and D. Herschlag, *Methods Enzymol.*, 2009, **468**, 91–106.

66 K. Zheng, F. Liu, X. M. Xu, Y. T. Li, Z. Y. Wu and C. W. Yan, *New J. Chem.*, 2014, **38**, 2964–2978.

67 Y. Gilad and H. Senderowitz, *J. Chem. Inf. Model.*, 2014, **54**, 96–107.

68 D. Agudelo, P. Bourassa, M. Beauregard, G. Berube and H. A. T. Riahi, *PLoS One*, 2014, **8**, e69248.

69 (*a*) J. Marmur, *J. Mol. Biol.*, 1961, **3**, 208–218; (*b*) K. A. Meadows, F. Liu, J. Sou, B. P. Hudson and D. R. McMillin, *Inorg. Chem.*, 1993, **32**, 2919–2923.

70 K. A. Meadows, F. Liu, J. Sou, B. P. Hudson and D. R. McMillin, *Inorg. Chem.*, 1993, **32**, 2919–2923.

71 G. M. Sheldrick, *Acta Crystallogr.*, 2015, **C71**, 3–8.

72 A. L. Spek, *PLATON Procedure, A Multipurpose Crystallographic Tool*, Utrecht University, Utrecht, The Netherlands, 1998.

73 (*a*) F. Arjmand, M. Muddassir, Y. Zaidi and D. Ray, *MedChemComm*, 2012, **4**, 394–405; (*b*) J. R. Lakowicz and G. Webber, *Biochemistry*, 1973, **12**, 4161–4170.

74 M. A. Spackman and D. Jayatilaka, *CrystEngComm*, 2009, **11**, 19–32.

75 (*a*) D. Mustard and D. W. Ritchie, *Proteins*, 2005, **60**, 269–274; (*b*) G. Macindoe, L. Mavridis, V. Venkatraman, M. D. Devignes and D. W. Ritchie, *Nucleic Acids Res.*, 2010, **38**, 445–449.

76 T. Lammers, P. Peschke, V. Ehemann, J. Debus, B. Slobodin, S. Lavi and P. Huber, *Mol. Cancer*, 2007, **6**, 65–78.